Measurement of Rayleigh Scattering in Liquid Argon at Vacuum Ultraviolet Wavelengths

Larry Zhao[1]
Fermi National Accelerator Laboratory, SULI Intern

(*Electronic mail: zhao_larry@berkeley.edu.)

(Dated: 11 August 2023)

Liquid argon based detectors are limited in scintillation light analysis capabilities due to inconsistent measurements of fundamental constants essential for reconstruction of scintillation events. This experiment measures the Rayleigh scattering length of vacuum ultraviolet light propagating in liquid argon in support of liquid argon experiments. Preliminary results are presented for the Rayleigh scattering length in a range of vacuum ultraviolet wavelengths. Current data collection and analysis methods in this measurement require advancements to understand and eliminate anomalous phenomena in the data. Future measurements in this experiment aim to precisely measure the liquid argon ultraviolet light attenuation. Results will contribute to the development of new photon system analysis methods for liquid argon experiments.

I. INTRODUCTION

In this measurement, we aim to directly measure the attenuation from Rayleigh scattering in a wide range of vacuum-ultraviolet (VUV) wavelengths in liquid argon. This measurement will support the advancement of scintillation photon analysis in liquid argon time projection chambers (LArTPCs) and innovate new error reduction capabilities for neutrino experiments such as DUNE and SBND as well as dark matter experiments such as DarkSide.

A. Background

The Deep Underground Neutrino Experiment (DUNE)[1] primary physics objectives are to conduct precision measurements of long baseline neutrino oscillations, observe neutrinos from rare galactic supernovas, and potentially discover nucleon decays. The precision oscillation measurement aims to answer major neutrino physics questions such as the ordering of neutrino masses, the existence of potential CP violation in the lepton sector, and if the neutrino mixing matrix is unitary. Neutrinos produced by a supernova event creates rare opportunities to study astroparticle physics in extreme environments where neutrino-neutrino interactions may be measured. Observing nucleon decays would be a major discovery and advance beyond the standard model physics.

DUNE consists of the Long Baseline Neutrino Facility (LBNF) and a near detector at Fermilab, as well as a far detector located underground at the Homestake Mine in South Dakota. The LBNF produces a high intensity neutrino beam and the initial beam composition is measured by the near detector in support of the long baseline neutrino oscillation measurement. The far detector measures the neutrino beam spectrum after oscillations, detects potential supernova neutrinos, and searches for nucleon decays. The far detector consists of four time projection chambers (TPCs) containing 40 kilotons of liquid argon in total.

Liquid argon is an excellent scintillating medium because it produces a large amount of scintillation light. The nominal 500 V/cm electric field design of DUNE produces 26,000 scintillation photons per MeV of deposited energy. At lower electric fields, even more scintillation light is emitted due to more ionized electrons recombining with argon ions. Argon is also relatively transparent to its own scintillation light because light emission requires the dissociation of dimers formed by excited argon atoms, which are generally not present to reabsorb the propagating photons. The argon scintillation light spectrum is a narrow peak centered at 128 nm in the vacuum ultraviolet wavelength regime.

In TPCs, a charged particle ionizes the argon atoms, an applied electric field causes the ionized charge to drift towards the anode in a time span of milliseconds, and readout wires or planes record the detected charge pattern in space in two dimensions while the drift time reconstructs the third dimension. Of the energy deposited by particles, $\sim$40% produces ionized drift electrons and $\sim$60% produces scintillation light. Scintillation light does not provide fine spatial resolution of signals, but is still critical to measuring the third spatial dimension. Reconstructing the absolute position where particles pass through the volume requires knowing the time difference in arrival between scintillation light (time from emission to detection of order nanoseconds) and ionization drift electrons (velocity of 1 mm/μs). This is the only measurement of the absolute time for reconstruction of absolute position in non-beam events such as supernova neutrinos and nucleon decays. The absolute position is key to defining fiducial volumes to exclude background signals and correct for the attenuation of charge signals in flight.

B. Motivation

Though the scintillation photon detector system primarily functions to reconstruct position information, it can also advance DUNE's physics goals further by enabling a second calorimetric measurement of the total event energy. The addition of an alternative energy measurement improves analysis by increasing energy resolution (since the photon and charge energy measurements resolution have different limita-

tions), as well as provide a cross check of the energy measurement, allowing for reductions in the systematic uncertainty. The improved analytical sensitivity can contribute to DUNE's physics objectives, and gains in systematic uncertainty reduction are particularly important for measurements of small oscillation effects. However, developing this new application of the photon detector system requires fundamental measurements to accurately reconstruct the deposited energy from scintillation photons. Critically, there is no consensus on the total attenuation and Rayleigh scattering length of scintillation photons propagating in liquid argon.

The total attenuation length L is related to absorption length L_A and scattering length L_S by

$$\frac{1}{L} = \frac{1}{L_A} + \frac{1}{L_S} \tag{1}$$

where we expect the total attenuation length to be largely dominated by Rayleigh scattering. For measurements at different wavelengths and liquid argon depths, the Rayleigh scattering ratio R at 90°is

$$R = \frac{I}{I_0}\frac{r^2}{V} \propto \frac{1}{\lambda^4} \tag{2}$$

where I is the scattered intensity, I_0 is the incident intensity, r is distance from the scattering center to the detector, and V is the scattering volume.

Experiments such as Ishida et al[2] measured the attenuation length of $\lambda = 128$ nm photons in liquid argon to be 66 ± 3 cm. Neumeier et al[34] then measured an attenuation length of 1.63 m, and subsequently established a lower bound of 1.1 m. Later, M. Babicz et al[56] derived a Rayleigh scattering length of 91.0 ± 2.3 cm and then 99.1 ± 2.3 cm from measurements of $\lambda = 128$ nm photon velocity in liquid argon.

In addition, Neumeier et al[3] found that the VUV photon attenuation length in liquid argon is not described by a single universal value due to wavelength dependent emission and absorption. They also reported absorption and emission line effects due to the presence of oxygen, water, and xenon contamination. Other impurities such as nitrogen also impact liquid argon measurements, as reported by the WArP collaboration[7] and Jones et al[8].

Calculations by Seidel, Lanou, and Yao[9] yielded a 90 cm scattering length, while Grace et al[10] calculated a 55 ± 5 cm scattering length. The disparity in the scattering length calculation is attributed to the required extrapolation of properties of liquid argon from longer wavelengths and sometimes from gas to liquid. The factor of three variation in previous Rayleigh scattering length experiments and calculations requires further investigation to determine the true scattering length.

II. EXPERIMENTAL DESIGN

A. Experimental Setup

The Noble Liquid Test Facility (NLTF) in the Proton Assembly Building (PAB) at Fermilab offers extensive research and development infrastructure for optical tests in ultra pure liquid argon. The scintillation photon attenuation measurement in liquid argon is conducted using the TallBo cryostat (Fig. 1) situated at the NLTF.

(a) TallBo Cryostat

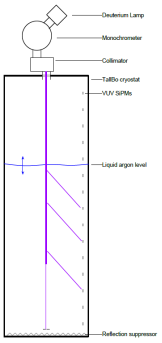

(b) Cryostat Diagram

FIG. 1: TallBo Cryostat

A deuterium lamp installed above the cryostat produces a light spectrum, which includes the ultraviolet wavelength range of interest. The deuterium lamp spectrum is reduced to a narrow wavelength band by a monochromator. The resulting light is collimated by a collimator so the photons travel in parallel, thus reducing beam divergence and refracted light inside the cryostat. Finally, the monochromatic photon beam enters the cryostat perpendicular to the liquid argon surface below. Reflection suppressors line the bottom and sides of the cryostat to prevent detection of reflected photons.

Silicon photomultiplier (SiPM) photodetectors measure the photon signals incident upon its active area. Ten Hamamatsu VUV4 S13370-6050CN 6×6 mm^2 SiPMs (numbered channels 0 to 9) are installed at strategic positions on the bottom (channel 0 and 1) and side (channel 2 to 9, in order from bottom to top) of the cryostat to collect scattered photons. This SiPM model is sensitive to photons down to $\lambda = 120$ nm[11], removing the requirement of wavelength shifting coatings used in experiments with previous generations of SiPMs. A SiPM Signal Processor (SSP) applies the SiPM bias voltages, sets trigger thresholds for data collection, converts analog SiPM signals to digital values, and analyzes the data. LBNEWare software interfaces with the SSP and is used for applications such as controlling the SiPM bias voltage and signal trigger threshold settings, inputting values related to the signal data collection and analysis parameters, as well as displaying recorded waveform signals.

The TallBo cryostat possesses a calibrated level meter to determine the liquid argon depth. Gas analyzers for nitrogen, oxygen, and water are used to confirm the liquid argon purity inside the cryostat. Other sensors monitor the temperature and vacuum pressure inside the cryostat.

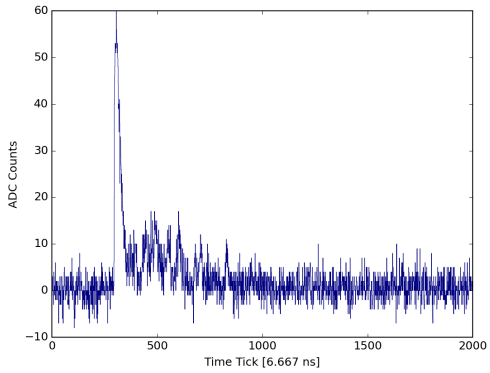

FIG. 2: Example SiPM Signal Waveform

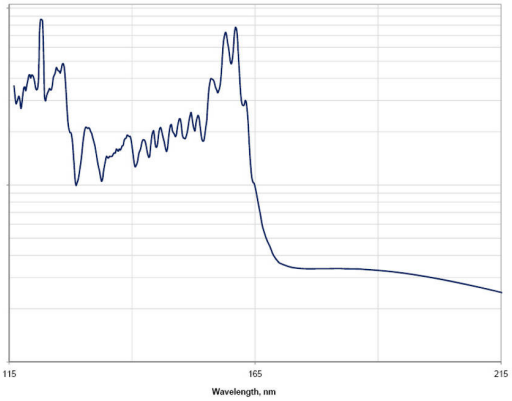

FIG. 3: McPherson Deuterium Lamp Spectrum[12]

B. Procedure

First, we fill the cryostat with liquid argon to the maximum fill level and submerge the SiPMs. The SiPM detector response depends on the temperature, thus only SiPMs submerged in liquid argon are used for characterization of signal behavior. Of the installed SiPMs, channels number 1, 2, 4, and 5 are operated for the measurement. SiPM signal waveforms (Fig. 2) exceeding the trigger threshold are processed and recorded in output files. The SiPM dark signal rate at liquid argon cryogenic temperatures is standardized to ∼100 Hz for each SiPM by setting the trigger thresholds to the same values and tuning the applied bias voltages. Current inputs are set at an arbitrary value of 20 for the leading edge discriminator threshold, and a range from 43.80 to 44.22 V for the SiPM bias voltages.

Initial data collection procedures used Python commands to alternate between shutter closed and shutter open states in 1 second intervals. For each shutter open period, we also incremented the monochromator to a new wavelength. However, data collection using this procedure resulted in multiple unforeseen issues. First, the Arduino device generating regular electronic pulses to sync the computer and SSP timestamps did not interact correctly with the SSP in addition to causing grounding problems. Attempted solutions, such as using a TTL/NIM converter to rectify the Arduino signal, also failed to reliably synchronize the Arduino and SSP pulses. Second, operating the monochromator motor power supply caused anomalous responses in the SiPM waveforms, likely due to grounding issues. As a result, later data collection runs exclude operation of the Arduino, SSP sync, and monochromator motor. Third, the LBNEWare software limits data collection to 50,000 triggers per run, so we cannot collect data for the entire wavelength range in one run. Furthermore, data transfer via USB cable from the SSP to the computer saturates easily, so we disabled recording waveform data to only save the SSP calculated values and scan one wavelength per run.

The results from testing initial procedures informed the methods developed for the current data collection procedure. For each liquid level in a data collection run, 50,000 SiPM dark signals are measured to quantify the background due to dark counts, cosmic ray scintillations (e.g. cosmic muons), and radioactive decays (e.g. argon isotopes like ^{38}Ar). The monochromator is then set to the desired single wavelength, the shutter is opened to measure photons, before LBNEWare and the SSP record 50,000 triggers. Next, we repeat the shutter open measurement with the monochromator set to the next wavelength. We scan the wavelength range from 124 nm to 180 nm, encompassing both the liquid argon and liquid xenon scintillation wavelengths of 128 and 175 nm, respectively. We note that the data rate saturates at certain wavelengths (e.g. 160 nm) due to intense peaks in the deuterium lamp spectrum (Fig. 3). The dark signals are then measured a second time to determine the background rate variation across the run. The liquid level is lowered, and the wavelength scan measurement procedure is repeated for each liquid level.

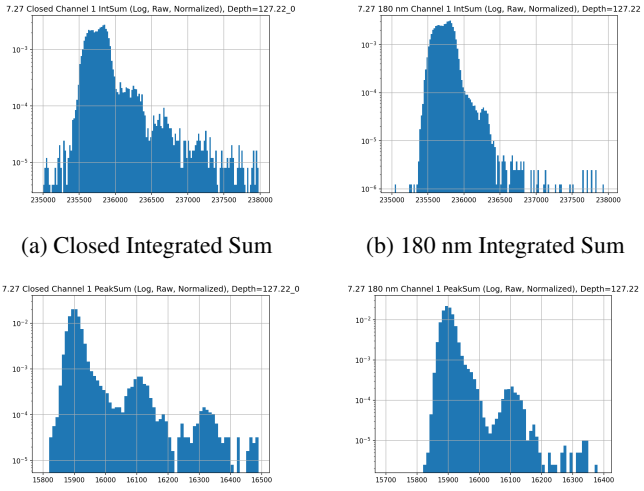

(a) Closed Integrated Sum

(b) 180 nm Integrated Sum

(c) Closed Peak Sum

(d) 180 nm Peak Sum

FIG. 4: Waveform Analysis Histograms

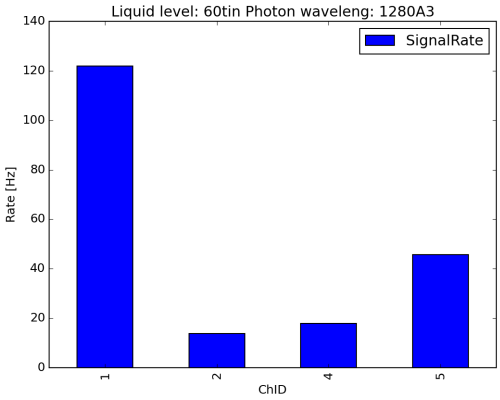

FIG. 5: Background Subtracted Rates (127.22 cm depth)

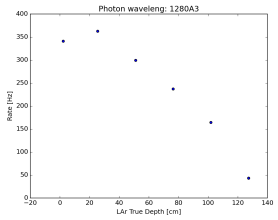

(a) 128 nm Rate (Background Subtraction)

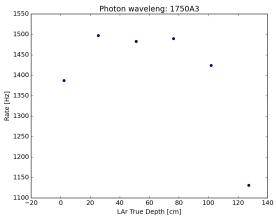

(b) 175 nm Rate (Background Subtraction)

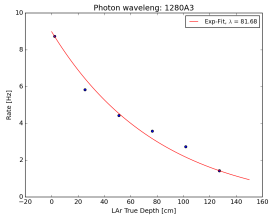

(c) 128 nm Rate (Background Division)

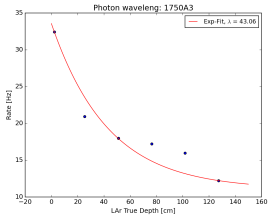

(d) 175 nm Rate (Background Division)

FIG. 7: Rate Analysis

III. ANALYSIS

Initial data analysis studies supported optimization of data collection settings as well as analysis techniques. Investigating the waveform and SSP calculated values for integrated sum (sum of a tunable number of waveform values in the peak) and peak sum (sum of a tunable number of waveform values in a subset of the peak) with no background subtraction indicates that a single trigger event generally corresponds to one incident photon (Fig. 4). The majority of integrated sum and peak sum values are distributed around a central value. A smaller number of events are distributed around a higher value (below the high energy background signal peaks), consistent with cross-talk between SiPM pixels. As a result, we expect the number of low energy trigger events to be equal to the number of light source photons detected.

We expect the largest number of scattered photon signals on the SiPMs close to the liquid argon surface because the light intensity is greatest at the beam point of entry. As a result, more light is available for scattering near the liquid surface compared to at greater depths. (Fig. 5) corroborates the expected trend, but does not match expected numerical proportions from simulation results. As a result, we compare signals in a single channel at different liquid levels, instead of comparing signals between different channels at a single liquid level.

To account for differences in time length between runs, we use background subtracted trigger rate ((Trigger Number – Background Number)/Run Time Length) as the primary analysis metric. The background rates display small variations over time, but more significantly depend on liquid level (Fig. 6). Lower background rates at lower liquid levels are explained by less scintillation signal rates in the smaller volume from cosmic rays (e.g. atmospheric muons) and radioactive decays of argon isotopes (e.g. ^{38}Ar).

The measured VUV light decreases exponentially as the liquid level lowers because of the relation between beam attenuation versus depth. (Fig. 7) displays selected results at the liquid argon and liquid xenon scintillation wavelengths in

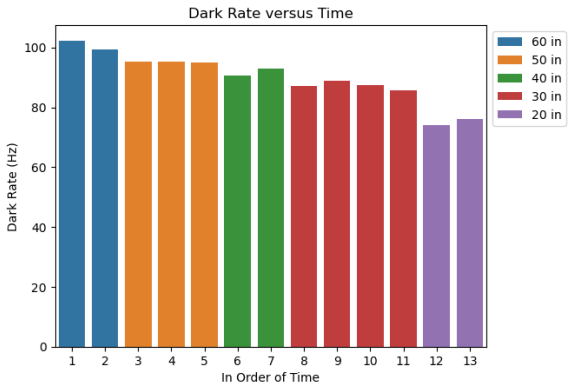

FIG. 6: Dark Rate vs Liquid Level

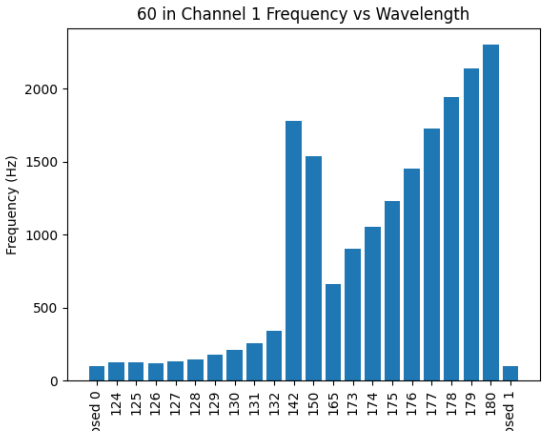

FIG. 8: Rate versus Wavelength (127.22 cm)

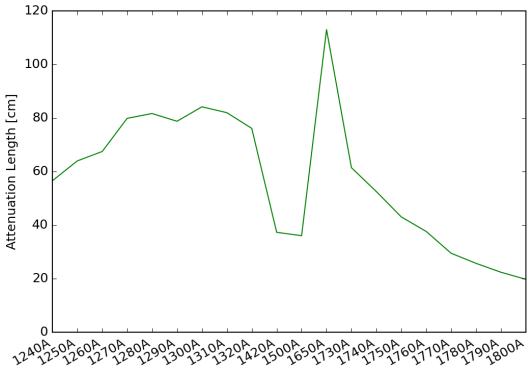

FIG. 9: Preliminary Rayleigh Scattering Length versus Wavelength

liquid lowering data runs. We observe anomalous responses in the background subtracted plots, where attenuation behavior is inconsistent with exponential decay versus liquid level across the wavelength spectrum. Dividing the signal rate by the background instead of subtracting yields a more evident relation to an exponential structure, but the mechanism causing division to be superior to background subtraction is not yet understood.

The total photon rate across the wavelength range demonstrates reasonable behavior (Fig. 8) when accounting for the deuterium emission spectrum (Fig. 3), the SiPM detection efficiency[11], and the relation given in (Eq. 2). Investigating integrated sum and peak sum indicates the multi photon (greater than second lowest peak or 3PE) event rate is roughly constant (Tab. I), indicating those triggers are most likely a constant background from cosmic rays and radioactive isotope decays. As a result, we expect the number of trigger events in the first two Integrated Sum and Peak Sum peaks (Fig. 4) to be equal to the number of photons detected. This result informs further analysis methods to identify background signal sources and improve analysis of trigger rates.

IV. CONCLUSIONS

Preliminary data results in an initial measurement for Rayleigh scattering length at wavelengths from 124 to 180 nm (Fig. 9). However, the data and analysis produces results that we cannot yet explain. We do not observe the expected exponential relationship between background subtracted signal rates at different liquid levels, while background divided signal rates appear more exponential and suggest unknown mechanisms in the electronics or measurement setup. In addition, the latter analysis curve fitting still results in poor measures of goodness of fit. We then investigate these anomalous observations by analyzing the integrated sum and peak sum data, which indicate further cuts are needed to remove background signals.

A. Future Objectives

Further investigations into analysis selections to identify background signals, understanding unexpected patterns in background subtracted photon rates, and explaining other unknown phenomena are required. More data runs will take place in the Fall of 2023 to continue investigating solutions and conclude measurement results.

Acknowledgements: Alex Himmel and Wei Mu contributed greatly to work presented in this paper. Alex Himmel conceived and designed the experiment, then secured funding for equipment and personnel to conduct the measurement. Alex Himmel and Wei Mu were instrumental in commissioning the experiment, optimizing hardware and software setups, collecting data, and developing analysis methods. Wei Mu also contributed Figures 2, 5, 7, and 9 in this paper.

[1] A. I. Himmel, "Seeing Neutrinos: The Physics Potential of Photon Signals in DUNE,".
[2] N. Ishida et al., "Attenuation length measurements of scintillation light in liquid rare gases and their mixtures using an improved reflection suppresser," Nucl. Instr. and Meth. in Phys. Res. A **384**, 380–386 (1997).
[3] A. Neumeier et al., "Attenuation of vacuum ultraviolet light in liquid argon," Eur Phys. J. C **72** (2012).
[4] A. Neumeier et al., "Attenuation of vacuum ultraviolet light in pure and xenon-doped liquid argon - an approach to an assignment of the near-infrared emission from the mixture," EPL **111** (2015).
[5] M. Babicz et al., "Experimental study of the propagation of scintillation light in liquid argon," Nuclear Inst. and Methods in Physics Research, A **936**, 178–179 (2019).
[6] M. Babicz et al., "A measurement of the group velocity of scintillation light in liquid argon," JINST **15** (2020).
[7] R. Acciarri et al., "Effects of nitrogen contamination in liquid argon," JINST **5** (2010).
[8] B.J.P. Jones et al., "A measurement of the absorption of liquid argon scintillation light by dissolved nitrogen at the part-per-million level," JINST **8** (2013).
[9] G.M. Seidel, R.E. Lanou, W. Yao, "Rayleigh scattering in rare-gas liquids," Nuclear Instruments and Methods in Physics Research Section A **489**, 189–194 (2002).
[10] E. Grace et al, "Index of refraction, rayleigh scattering length, and sellmeier coefficients in solid and liquid argon and xenon," Nuclear Inst. and Methods in Physics Research, A **867**, 204–208 (2017).
[11] *VUV-MPPC 4th generation (VUV4) Product Flyer*, Hamamatsu (2017).
[12] *Deuterium Source with Magnesium Fluoride Window*, McPherson (2017).

Appendix A: Appendixes

TABLE I: Total and Third Peak Sum Peak Trigger Rate for Channel 1 and Channel 2

Wavelength	Ch 1 Rate 3PE	Ch 1 Total Rate	Ch 2 Rate 3PE	Ch 2 Total Rate
Closed	1.114702098	102.3247707	0.7404225613	100.5428746
124	1.056804038	125.4932594	0.8170249709	103.5579151
125	0.9924281097	122.3936118	0.8255596665	104.4420804
126	1.056945719	120.9897121	0.7512176188	102.445119
127	1.069047503	129.7556406	0.6859721475	103.6174292
128	1.080057264	146.0730079	0.862150974	105.5708605
129	0.9905293452	174.7768394	0.846077149	109.0923622
130	1.077132777	209.2245382	0.7596620637	111.6589851
131	1.251333603	256.4475502	0.8595018687	116.3866648
132	0.8422378213	339.6775213	0.9475175489	124.5007979
142	1.142222238	1777.959089	0.9017543985	322.5876068
150	0.3041595671	1540.203216	0.851646788	421.4434962
165	1.069427662	662.8983661	0.8807051332	123.8858554
173	1.168730067	904.3373543	0.9349840538	126.9240853
174	1.147285162	1057.149733	0.7648567748	135.114891
175	1.159506982	1232.191506	1.026991899	141.0954354
176	1.597352275	1453.400409	0.8367083346	147.5268923
177	1.502471773	1728.107681	0.6628551941	155.3732575
178	1.270036225	1944.327766	1.074646037	162.6134844
179	1.761626362	2142.671482	0.5338261702	174.1340967
180	1.252850075	2301.884222	0.5694773068	178.5311357
Closed	1.125053412	99.22346065	0.7656613499	99.02032601